

# 3-D Numerical Modeling for the Magnetization of Superconductors Using a Local Discontinuous Galerkin Finite Element Method

Yann-Meing Law<sup>1</sup>, Damien Tageddine, and Steven Dufour<sup>1</sup>

Département de mathématiques et de génie industriel, École Polytechnique de Montréal, Montreal, QC H3T 1J4, Canada

A numerical methodology is proposed to discretize a nonlinear low-frequency approximation to Maxwell's equations using a local discontinuous Galerkin (DG) finite element method, with an upwind-like numerical flux, for modeling superconductors. In this paper, we focus on high-temperature superconductors (HTS) and the electrical resistivity is modeled using a power law. Nodal elements and the Whitney element are used. Numerical studies have been performed to verify the proposed methodology: a problem with a manufactured solution, the nonlinear magnetic front problem, and the magnetization of HTS wires. Based on the final time that can be reached for a given time-step size, the proposed strategy is compared with the  $\mathbf{H}$  formulation discretized using the Galerkin finite element method with the Whitney element for the magnetic front problem. The proposed local DG strategy allows the use of a larger time-step size over a longer time interval, particularly, when we use the Whitney element. The proposed methodology can also capture sharp gradients of the current density with limited spurious oscillations. The numerical results are in agreement with Bean's model for large values of power-law's exponent. The proposed local DG strategy could be generalized to more complex electrical resistivity models, including multiphysics models.

**Index Terms**—Local discontinuous Galerkin (DG) finite element method, low-frequency Maxwell's equations, magnetization, nonlinear resistivity,  $p$ -curl problem, power-law model, superconductors.

## I. INTRODUCTION

NUMERICAL modeling of high-temperature superconductors (HTS) involves the discretization of Maxwell's equations, in low-frequency regime, using a power law to model electrical resistivity. Most numerical strategies are based on a modification of Maxwell's equations in order to obtain a parabolic problem expressed with respect to the magnetic field [1], the electric field [2], the magnetic vector potential and a scalar potential [3], or the current vector potential and the magnetic scalar potential [4]. There exist many commercial codes that allow the discretization of these formulations. Various discretization methods, such as the finite difference method [2], [5] and the finite element method [1], [6], are used to discretize the parabolic problems.

These parabolic problems are known to develop sharp gradients of the current density for large values of the exponent of the power-law model [7], [8]. These gradients are difficult to capture using numerical methods designed to discretize parabolic partial differential equations (PDEs). Moreover, small time-step sizes must be used to guarantee the stability of the discrete problem. They make computational costs associated with the study of industrial problems prohibitive [9].

The discontinuous Galerkin (DG) finite element method, for which discontinuous discrete solutions are allowed, is better suited for capturing sharp solutions. The DG finite element method is used to discretize linear low-frequency approximations to Maxwell's equations [10]–[12] and nonlinear Maxwell's equations to study nonlinear optics prob-

lems [13]–[15]. For HTS modeling, Kameni *et al.* [6], [16] and Makong *et al.* [17] use the nodal DG finite element method to discretize the parabolic formulation based on the electric field, also known as the  $\mathbf{E}$  formulation. They use the nonsymmetric interior penalty (NIP) method for the numerical flux, which depends on a positive parameter that needs to be determined. The NIP method enforces the continuity of the discrete-dependent variable and its gradient at the interface between elements. Since the boundary conditions are usually given in term of the magnetic field, the imposition of these conditions with the  $\mathbf{E}$  formulation is not direct. Recently, Makong *et al.* [18] discretize the parabolic problem with respect to the magnetic field, the  $\mathbf{H}$  formulation, using the nodal DG method with the symmetric interior penalty (SIP) method as numerical flux. The SIP method enforces the continuity of the tangential component of the discrete magnetic field. Both numerical methodologies have taken advantage of the natural parallelization of the DG method to reduce the computational time of large-scale tridimensional problems.

In this paper, we work directly with a low-frequency approximation to Maxwell's equations composed of a system of the first-order PDEs, namely, Faraday's law and Ohm's law, similar to what is proposed by Law and Laforest [5] for HTS modeling in the context of the finite-difference time-domain method. The benefit to use this form of Maxwell's equations in low-frequency regime is to split the nonlinear PDE into a linear and nonlinear part, i.e., respectively, Faraday's law and Ohm's law. A linear upwind-like numerical flux for this nonlinear problem is proposed using the continuous inverse function of Ohm's law. The proposed numerical methodology can be generalized to more complex and multiphysics electrical resistivity models as long as there is a continuous inverse function of Ohm's law. Examples of such models can be found in [19].

Manuscript received November 8, 2018; revised January 25, 2019; accepted March 16, 2019. Date of publication April 25, 2019; date of current version July 18, 2019. Corresponding author: Y.-M. Law (e-mail: yann-meing.law-kam-cio@polymtl.ca).

Color versions of one or more of the figures in this paper are available online at <http://ieeexplore.ieee.org>.

Digital Object Identifier 10.1109/TMAG.2019.2907665

This paper is structured as follows. In Section II, a low-frequency approximation to Maxwell's equations for modeling HTS problems with a nonlinear electrical resistivity is first introduced. This formulation is discretized using a local DG finite element method with a linear upwind-like numerical flux in Section III. We consider standard nodal elements and the Whitney element. The Whitney element, which is the lowest-order Nédélec element, is known to be at divergence-free locally and, therefore, is used to enforce locally the divergence-free magnetic induction field constraint. A brief review of the discretization of the  $\mathbf{H}$  formulation using the Galerkin finite element method (GFEM) with the Whitney element is also done. This numerical strategy is popular in the electrical engineering community. To the best of our knowledge, only this strategy is used for modeling industrial systems with complex geometries in three dimensions [20], [21]. In Section IV, a problem with a manufactured solution, the nonlinear magnetic front problem, and the magnetization of HTS wires are studied to verify the proposed methodology. Based on the final time that can be reached for a given time-step size, the nonlinear magnetic front problem is also used to compare the proposed local DG strategy with the  $\mathbf{H}$  formulation discretized using the GFEM-based strategy. For the magnetization of HTS wires, we complicate the problem by considering air medium around the HTS wire.

## II. MAXWELL'S EQUATIONS IN THE LOW-FREQUENCY REGIME FOR HTS MODELING

Assuming a linear medium, electromagnetic phenomena are modeled using Maxwell's equations

$$\begin{aligned}\partial_t \mathbf{B} + \nabla \times \mathbf{E} &= 0 \\ \partial_t \mathbf{D} - \nabla \times \mathbf{H} &= -\mathbf{J} \\ \nabla \cdot \mathbf{D} &= \rho_c \\ \nabla \cdot \mathbf{B} &= 0\end{aligned}\quad (1)$$

where  $\mathbf{B}$  is the magnetic induction field,  $\mathbf{E}$  is the electric field,  $\mathbf{D} = \epsilon \mathbf{E}$  is the electric field displacement,  $\mathbf{H} = \mu^{-1} \mathbf{B}$  is the magnetic field,  $\rho_c$  is the electric charge density,  $\epsilon$  is the electric permittivity,  $\mu$  is the magnetic permeability, and  $\mathbf{J}$  is the current density. The relationship between the electric field  $\mathbf{E}$  and the current density  $\mathbf{J}$  is given by Ohm's law

$$\mathbf{E} = \rho \mathbf{J} \quad (2)$$

where  $\rho$  is the electrical resistivity. Assuming a low-frequency regime, we have  $\|\partial_t \mathbf{D}\|_2 \ll \|\mathbf{J}\|_2$ , where  $\|\cdot\|_2$  is the Euclidean norm, which leads to the magneto-quasi-static condition  $\partial_t \mathbf{D} \approx 0$  [22]. The current density is then given by Ampère's law

$$\mathbf{J} = \nabla \times \mathbf{H} \quad (3)$$

and Ohm's law (2) becomes

$$\mathbf{E} = \rho \nabla \times \mathbf{H}. \quad (4)$$

The first equation of system (1), which is known as Faraday's law, with Ohm's law (4) and the divergence-free

constraint on  $\mathbf{B}$  gives the system of the first-order PDEs

$$\begin{aligned}\partial_t(\mu \mathbf{H}) + \nabla \times \mathbf{E} &= 0 \\ \mathbf{E} - \rho \nabla \times \mathbf{H} &= 0 \\ \nabla \cdot (\mu \mathbf{H}) &= 0\end{aligned}\quad (5)$$

which are known as Maxwell's equations in the low-frequency regime for conducting materials. By combining the first and second equation of system (5), a parabolic problem expressed with respect to the magnetic field  $\mathbf{H}$  is obtained

$$\begin{aligned}\partial_t(\mu \mathbf{H}) + \nabla \times (\rho \nabla \times \mathbf{H}) &= 0 \\ \nabla \cdot (\mu \mathbf{H}) &= 0\end{aligned}\quad (6)$$

which is known as the  $\mathbf{H}$  formulation. It consists of a parabolic PDE with a divergence-free constraint on  $\mu \mathbf{H}$ . In this paper, we assume that  $\mu$  is a constant, and therefore, we have to satisfy  $\nabla \cdot \mathbf{H} = 0$ .

Let us consider a domain  $\Omega$  and its boundary  $\Gamma$ . Assuming the boundary  $\Gamma = \Gamma_D \cup \Gamma_N$  to be such that  $\Gamma_D \neq \emptyset$  and  $\Gamma_D \cap \Gamma_N = \emptyset$ , the boundary conditions for system (6) are given by

$$\mathbf{n} \times \mathbf{H} = \mathbf{G}_1 \quad \text{on } \Gamma_D \times I \quad (7)$$

$$\mathbf{n} \times \mathbf{E} = \mathbf{G}_2 \quad \text{on } \Gamma_N \times I \quad (8)$$

where  $\mathbf{E}$  is given by Ohm's law (4),  $\mathbf{n}$  is the outward unit normal to the boundary  $\Gamma$ , and  $I = [t_0, t_f]$  is a time interval. The dependent variables for system (5) are both the magnetic field  $\mathbf{H}$  and the electric field  $\mathbf{E}$ , and boundary conditions (7) and (8) can, therefore, be imposed on all  $\Gamma$ .

For high-temperature superconducting materials, the electrical resistivity is modeled using the power law

$$\rho = \frac{E_c}{J_c^p} \|\nabla \times \mathbf{H}\|_2^{p-1} \quad (9)$$

where  $E_c$  is the amplitude of the electric field for the critical current,  $J_c$  is the critical current density, and  $p > 1$  is a parameter [23], [24]. The first equation of system (6) with power-law model (9) gives

$$\partial_t(\mu \mathbf{H}) + \nabla \times \left( \frac{E_c}{J_c^p} \|\nabla \times \mathbf{H}\|_2^{p-1} \nabla \times \mathbf{H} \right) = 0 \quad (10)$$

which is also known as the  $p$ -curl problem [25]. The nonlinear parabolic equation (10) becomes an ordinary differential equation for  $\nabla \times \mathbf{H} = 0$ , i.e.,  $\partial_t(\mu \mathbf{H}) = 0$ . The  $p$ -curl problem is, therefore, degenerated. By taking the limit as  $p \rightarrow \infty$  in power-law model (9), Bean's model is obtained

$$\|\mathbf{E}\|_2 = \begin{cases} 0 & \text{if } \|\mathbf{J}\|_2 < J_c \\ e & \text{if } \|\mathbf{J}\|_2 = J_c \end{cases} \quad (11)$$

where  $e \in [0, \infty[$  [26]. For simple geometries, such as a cylinder, analytical solutions with discontinuities on the current density  $\mathbf{J}$  are known. They are used to verify numerical strategies for large exponents  $p$ .

### III. NUMERICAL METHODOLOGY

As mentioned earlier, most numerical strategies used to study HTS problems modify the low-frequency approximation to Maxwell's equations (5) into a parabolic problem. In this section, we briefly review the classical GFEM with the Whitney element to discretize the  $\mathbf{H}$  formulation (6). We also propose a local DG method to discretize the first two equations of system (5) for modeling HTS.

#### A. Galerkin Finite Element Method

Since the GFEM is based on the weak form of the PDEs, let us consider the space of square integrable functions

$$L_2(\Omega) = \{w : \Omega \rightarrow \mathbb{R} \text{ s.t. } \|w\|_{L_2(\Omega)} < \infty\}$$

where the  $L_2$ -norm is given by

$$\|w\|_{L_2(\Omega)} = \left( \int_{\Omega} w^2 d\Omega \right)^{1/2}$$

and  $\Omega$  is the domain of definition of the problem. For a vector field in  $[L_2(\Omega)]^3$ , the  $L_2$ -norm is given by

$$\|\mathbf{w}\|_{L_2(\Omega)} = \left( \sum_{i=1}^3 \|w_i\|_{L_2(\Omega)}^2 \right)^{1/2}. \quad (12)$$

The inner product in  $L_2(\Omega)$  is given by

$$(\mathbf{v}, \mathbf{w})_{\Omega} = \int_{\Omega} \mathbf{v} \cdot \mathbf{w} d\Omega$$

in  $\Omega$ . We also introduce the notation

$$(\mathbf{v}, \mathbf{w})_{\Gamma} = \int_{\Gamma} \mathbf{v} \cdot \mathbf{w} ds$$

for functions defined on the boundary  $\Gamma$  of  $\Omega$ . By multiplying the equations to be discretized by a test function  $\psi$  that belongs to a functional space  $\mathbf{W}$ , followed by an integration over  $\Omega$ , the weak form of the first equation of the  $\mathbf{H}$  formulation (6) is obtained

$$(\partial_t(\mu \mathbf{H}), \psi)_{\Omega} + (\nabla \times (\rho \nabla \times \mathbf{H}), \psi)_{\Omega} = 0, \quad \forall \psi \in \mathbf{W}.$$

Using the divergence theorem, the weak form becomes

$$\begin{aligned} & (\partial_t(\mu \mathbf{H}), \psi)_{\Omega} + (\rho \nabla \times \mathbf{H}, \nabla \times \psi)_{\Omega} \\ & = -(\mathbf{n} \times (\rho \nabla \times \mathbf{H}), \psi)_{\Gamma}, \quad \forall \psi \in \mathbf{W} \end{aligned}$$

where  $\mathbf{n}$  is the outward unit normal to  $\Gamma$ .

Let us consider the case where we have the Dirichlet boundary conditions (7) on all  $\Gamma$ . This leads us to work with

$$\mathbf{V} = \{\mathbf{H} \in H(\text{curl}, \Omega) : \mathbf{n} \times \mathbf{H} = \mathbf{G}_1 \text{ on } \Gamma\}$$

where

$$H(\text{curl}, \Omega) = \{\mathbf{v} \in [L_2(\Omega)]^3 : \nabla \times \mathbf{v} \in [L_2(\Omega)]^3\}$$

and

$$\mathbf{W} = \{\mathbf{v} \in H(\text{curl}, \Omega) : \mathbf{n} \times \mathbf{v} = 0 \text{ on } \Gamma\}.$$

We then have that

$$-(\mathbf{n} \times (\rho \nabla \times \mathbf{H}), \psi)_{\Gamma} = (\rho \nabla \times \mathbf{H}, \mathbf{n} \times \psi)_{\Gamma} = 0, \quad \forall \psi \in \mathbf{W}.$$

The weak problem associated with the  $\mathbf{H}$  formulation is then find  $\mathbf{H} \in \mathbf{V}$  such that

$$(\partial_t(\mu \mathbf{H}), \psi)_{\Omega} + (\rho \nabla \times \mathbf{H}, \nabla \times \psi)_{\Omega} = 0, \quad \forall \psi \in \mathbf{W}. \quad (13)$$

Let us now define a discrete functional space  $\mathbf{V}_h \subset \mathbf{V}$ . The discrete subspace associated with the Whitney element [27], also known as an edge element to electrical engineers, is a popular discrete subspace of  $H(\text{curl}, \Omega)$  for the discretization of the  $\mathbf{H}$  formulation [28]. It has been used to model HTS problems [29]. The Whitney element shape functions are locally divergence-free. The discrete magnetic divergence-free constraint is therefore only satisfied locally on each element [30].

The transient term  $\partial_t(\mu \mathbf{H})$  is discretized using a semi-discrete approach, where the second-order accurate backward-differentiation formula (BDF) scheme is used. The curl-curl matrix, given by the term  $(\nabla \times \psi, \nabla \times \psi)_{\Omega}$ , is known to be singular with the Whitney element [22], [31]. Time discretization makes the assembly matrix invertible. The discretization of problem (13) using the GFEM and the second-order accurate BDF scheme with nonlinear electrical resistivity is linearized using the following fixed-point iteration scheme, for each time step:

$$\begin{aligned} & (\mathbf{H}_h^{n,k+1}, \psi_h)_{\Omega} + \frac{3 \Delta t}{2 \mu} (\rho (\nabla \times \mathbf{H}_h^{n,k}) \nabla \times \mathbf{H}_h^{n,k+1}, \nabla \times \psi_h)_{\Omega} \\ & = \frac{1}{3} (4 \mathbf{H}_h^{n-1} - \mathbf{H}_h^{n-2}, \psi_h)_{\Omega} \end{aligned}$$

where  $\mathbf{H}_h^{n,k}$  is the  $k$ th fixed-point iteration of the discrete magnetic field at  $t_n$ ,  $\Delta t$  is the time-step size, and  $\psi_h$  is a discrete test function.

#### B. Local Discontinuous Galerkin Finite Element Method

Considering an initial condition of the magnetic field that satisfies the divergence-free constraint, it can be shown using Faraday's law that the magnetic field remains at divergence-free for all later time at the continuous level. A local DG finite element method is then used to directly discretize the first two equations of system (5). The system of equations is discretized element by element. For two elements  $K$  and  $K^*$  that share a common face, the jump of a variable  $v$  across the boundary of these elements is defined as  $[[v]] = v^+ - v^-$  where  $v^+$  belongs to element  $K$  and  $v^-$  belongs to  $K^*$ . We then define the space of piecewise polynomials as

$$D_h = \{w \in L_2(\Omega) : w|_K \in P_r(K), \forall K \in \Omega\}$$

where  $P_r(K)$  is the space of polynomials of degree  $r$  defined on  $K$ , and  $\mathbf{D}_h = [D_h]^3$ . For the Whitney element, we consider the following space:

$$\mathbf{D}_h = \{\mathbf{w} \in [L_2(\Omega)]^3 : \mathbf{w}|_K \in N_1(K), \forall K \in \Omega\}$$

where  $N_1(K)$  is the space spanned by the Whitney basis functions defined on  $K$ .

Let us consider the system of equations made of the first two equations of system (5) with a source term  $\mathbf{F}$ . For HTS,

the electrical resistivity is modeled using power law (9). The continuous inverse function of

$$\mathbf{E} = \rho(\nabla \times \mathbf{H}) \nabla \times \mathbf{H} = \frac{E_c}{J_c^p} \|\nabla \times \mathbf{H}\|_2^{p-1} \nabla \times \mathbf{H} \quad (14)$$

is given by

$$\nabla \times \mathbf{H} = \sigma(\mathbf{E}) \mathbf{E} = \begin{cases} \frac{J_c}{E_c^{1/p}} \|\mathbf{E}\|_2^{\frac{-p+1}{p}} \mathbf{E} & \text{if } \|\mathbf{E}\|_2 \neq 0 \\ 0 & \text{otherwise} \end{cases} \quad (15)$$

where  $\sigma(\mathbf{E}) = (J_c)/(E_c^{1/p}) \|\mathbf{E}\|_2^{(-p+1)/p}$  is the nonlinear conductivity, which goes to infinity as  $\|\mathbf{E}\|_2 \rightarrow 0$ . We, therefore, have

$$\begin{aligned} \partial_t(\mu \mathbf{H}) + \nabla \times \mathbf{E} &= \mathbf{F} \\ \sigma(\mathbf{E}) \mathbf{E} - \nabla \times \mathbf{H} &= 0. \end{aligned} \quad (16)$$

The discrete weak problem associated with system (16), defined on each element  $K$ , is then given by

$$\begin{aligned} (\partial_t(\mu \mathbf{H}_h), \mathbf{v}_h)_K + (\nabla \times \mathbf{E}_h, \mathbf{v}_h)_K &= (\mathbf{F}, \mathbf{v}_h)_K, \quad \forall \mathbf{v}_h \in \mathbf{D}_h \\ (\sigma(\mathbf{E}_h) \mathbf{E}_h, \mathbf{w}_h)_K - (\nabla \times \mathbf{H}_h, \mathbf{w}_h)_K &= 0, \quad \forall \mathbf{w}_h \in \mathbf{D}_h \end{aligned} \quad (17)$$

where  $\mathbf{H}_h$  is the discrete magnetic field,  $\mathbf{E}_h$  is the discrete electric field, and  $\mathbf{v}_h$  and  $\mathbf{w}_h$  are the associated discrete test functions. Using the divergence theorem twice, we have the additional terms

$$\langle \mathbf{n} \times (\mathbf{E}_h - \mathbf{E}_h^*), \mathbf{v}_h \rangle_{\partial K}$$

and

$$-\langle \mathbf{n} \times (\mathbf{H}_h - \mathbf{H}_h^*), \mathbf{w}_h \rangle_{\partial K}$$

defined on the boundary  $\partial K$  of  $K$  in the right-hand side of weak form (17). The term

$$\begin{bmatrix} -\mathbf{n} \times \mathbf{E}_h^* \\ \mathbf{n} \times \mathbf{H}_h^* \end{bmatrix}$$

is known as the numerical flux. The numerical flux is an approximation of the flux at the interface between the elements. Since system (16) is not hyperbolic from the missing transient term in the second equation of this system, an upwind-like numerical flux is, therefore, used like it is done for the discretization of the heat equation with a local DG method [32].

To find the expression of this numerical flux, let us first define  $\mathbf{U} = [\mathbf{H}^T \ \mathbf{E}^T]^T$  and  $\mathbf{G} = [\mathbf{F}^T \ 0^T]^T$ . We then rewrite system (16) as

$$Q \partial_t \mathbf{U} + A_1 \partial_x \mathbf{U} + A_2 \partial_y \mathbf{U} + A_3 \partial_z \mathbf{U} + K \mathbf{U} = \mathbf{G}. \quad (18)$$

We define the matrix

$$M = \sum_{i=1}^3 n_i A_i$$

where  $n_i$  is the  $i$ th component of the outward unit normal  $\mathbf{n}$  to  $\partial K$ . To find an upwind-like numerical flux, the matrix  $M$  is factorized as

$$M = R \Lambda R^{-1}$$

where the matrix  $\Lambda$  contains the eigenvalues of  $M$  and the matrix  $R$  contains the eigenvectors of  $M$ . The matrix  $\Lambda$  can be decomposed as  $\Lambda = \Lambda^+ + \Lambda^-$ , where the diagonal matrices  $\Lambda^+$  and  $\Lambda^-$  contain the positive and negative eigenvalues. Considering that the matrix  $\Lambda^-$  is responsible for making the information enter the element, and the matrix  $\Lambda^+$  is associated with the information leaving the element, the upwind-like numerical flux is chosen in such a way that

$$\begin{bmatrix} -\mathbf{n} \times \mathbf{E}_h^* \\ \mathbf{n} \times \mathbf{H}_h^* \end{bmatrix} = -R \Lambda^+ R^{-1} \mathbf{U}_h^+ - R \Lambda^- R^{-1} \mathbf{U}_h^-$$

where  $\mathbf{U}_h^+$  and  $\mathbf{U}_h^-$  are the discrete-dependent variables that belong, respectively, to  $K$  and  $K^*$ . We also have

$$\begin{bmatrix} \mathbf{n} \times (\mathbf{E}_h - \mathbf{E}_h^*) \\ -\mathbf{n} \times (\mathbf{H}_h - \mathbf{H}_h^*) \end{bmatrix} = R \Lambda^- R^{-1} \llbracket \mathbf{U}_h \rrbracket = \begin{bmatrix} \mathbf{F}_E \\ \mathbf{F}_H \end{bmatrix}$$

with

$$\begin{aligned} \mathbf{F}_E &= \frac{1}{2} (\mathbf{n} \times \llbracket \mathbf{E}_h \rrbracket - \llbracket \mathbf{H}_h \rrbracket) + (\mathbf{n} \cdot \llbracket \mathbf{H}_h \rrbracket) \mathbf{n} \\ \mathbf{F}_H &= \frac{1}{2} (-\mathbf{n} \times \llbracket \mathbf{H}_h \rrbracket - \llbracket \mathbf{E}_h \rrbracket) + (\mathbf{n} \cdot \llbracket \mathbf{E}_h \rrbracket) \mathbf{n} \end{aligned} \quad (19)$$

in a similar way to what is done in [33] and [32] for the first two equations of Maxwell's equations (1). The discrete weak problem is then: for each element  $K$ , find  $(\mathbf{H}_h, \mathbf{E}_h) \in \mathbf{D}_h \times \mathbf{D}_h$  such that

$$\begin{aligned} (\partial_t(\mu \mathbf{H}_h), \mathbf{v}_h)_K + (\nabla \times \mathbf{E}_h, \mathbf{v}_h)_K &= (\mathbf{F}, \mathbf{v}_h)_K + \langle \mathbf{F}_E, \mathbf{v}_h \rangle_{\partial K}, \quad \forall \mathbf{v}_h \in \mathbf{D}_h \\ (\sigma(\mathbf{E}_h) \mathbf{E}_h, \mathbf{w}_h)_K - (\nabla \times \mathbf{H}_h, \mathbf{w}_h)_K &= \langle \mathbf{F}_H, \mathbf{w}_h \rangle_{\partial K}, \quad \forall \mathbf{w}_h \in \mathbf{D}_h. \end{aligned} \quad (20)$$

*a) Better Conditioned Formulation Based on the Electrical Resistivity:* For HTS modeling, we do not use the weak form (20) with the nonlinear conductivity to stay away from any issue when  $\|\mathbf{E}\|_2 \rightarrow 0$ , such as ill-conditioned problem. By (14) and (15), we have that

$$\sigma(\mathbf{E}) \mathbf{E} - \nabla \times \mathbf{H} = 0$$

and

$$\mathbf{E} - \rho(\nabla \times \mathbf{H}) \nabla \times \mathbf{H} = 0.$$

Substituting the left-hand side of the second equation of the discrete problem (20) by  $(\mathbf{E}_h, \mathbf{w}_h)_K - (\rho(\nabla \times \mathbf{H}_h) \nabla \times \mathbf{H}_h, \mathbf{w}_h)_K$  gives the better conditioned discrete problem: for each element  $K$ , find  $(\mathbf{H}_h, \mathbf{E}_h) \in \mathbf{D}_h \times \mathbf{D}_h$  such that

$$\begin{aligned} (\partial_t(\mu \mathbf{H}_h), \mathbf{v}_h)_K + (\nabla \times \mathbf{E}_h, \mathbf{v}_h)_K &= (\mathbf{F}, \mathbf{v}_h)_K + \langle \mathbf{F}_E, \mathbf{v}_h \rangle_{\partial K}, \quad \forall \mathbf{v}_h \in \mathbf{D}_h \\ (\mathbf{E}_h, \mathbf{w}_h)_K - (\rho(\nabla \times \mathbf{H}_h) \nabla \times \mathbf{H}_h, \mathbf{w}_h)_K &= \langle \mathbf{F}_H, \mathbf{w}_h \rangle_{\partial K}, \quad \forall \mathbf{w}_h \in \mathbf{D}_h. \end{aligned} \quad (21)$$

The terms  $\langle \mathbf{F}_E, \mathbf{v}_h \rangle_{\partial K}$  and  $\langle \mathbf{F}_H, \mathbf{w}_h \rangle_{\partial K}$  can be seen as penalization terms on the jump of the dependent variables at the interface between the elements. Moreover, it can be shown that weak formulation (21) is equivalent to (20) when applied to  $\mathbf{H} \in [W^{1,1}(\Omega)]^3$  and  $\mathbf{E} \in [W^{1,1}(\Omega)]^3$ , where

$$W^{1,1}(\Omega) = \{v \in L^1(\Omega) : \partial_x v, \partial_y v, \partial_z v \in L^1(\Omega)\}$$

because we have  $[[\mathbf{H}]] = [[\mathbf{E}]] = 0$  for all triangular faces of the domain  $\Omega$  (cf., Lemma 1.23 in [33]). The penalization terms then become 0.

For non-superconducting material, one should also use weak formulation (21). The electrical resistivity  $\rho$  is small for a normal conducting material at HTS operating temperatures (about  $10^{-9}$   $\Omega\text{m}$  for copper). Considering that the conductivity  $\sigma = \rho^{-1}$ , the terms  $\partial_t(\mu \mathbf{H}_h)$ ,  $\nabla \times \mathbf{E}_h$ , and  $\nabla \times \mathbf{H}_h$  may then become negligible when compared to the term  $\sigma \mathbf{E}_h$  in discrete problem (20). This can also lead to an ill-conditioned problem.

Problem (21) discretized using the proposed local DG method and the second-order accurate BDF scheme, with the nonlinear electrical resistivity  $\rho(\nabla \times \mathbf{H})$ , is linearized using the following fixed-point scheme, for each time step and for each element  $K$ :

$$\begin{aligned} & (\mathbf{H}_h^{n,k+1}, \mathbf{v}_h)_K + \frac{3 \Delta t}{2 \mu} (\nabla \times \mathbf{E}_h^{n,k+1}, \mathbf{v}_h)_K \\ &= \frac{3 \Delta t}{2} (\mathbf{F}_E^n, \mathbf{v}_h)_K + \frac{3 \Delta t}{2 \mu} (\mathbf{F}_E^{n,k+1}, \mathbf{v}_h)_{\partial K} \\ & \quad + \frac{1}{3} (4 \mathbf{H}_h^{n-1} - \mathbf{H}_h^{n-2}, \mathbf{v}_h)_K \\ & (\mathbf{E}_h^{n,k+1}, \mathbf{w}_h)_K - (\rho(\nabla \times \mathbf{H}_h^{n,k}) \nabla \times \mathbf{H}_h^{n,k+1}, \mathbf{w}_h)_K \\ &= (\mathbf{F}_H^{n,k+1}, \mathbf{w}_h)_{\partial K} \end{aligned} \quad (22)$$

where  $\mathbf{F}_E^{n,k+1}$  and  $\mathbf{F}_H^{n,k+1}$  are the numerical flux evaluated using the  $(k+1)$ th iteration of the discrete magnetic field and the discrete electric field at  $t_n$ . A drawback of the DG methods is the associated number of degrees of freedom (DOFs). The total number of DOF associated with the proposed local DG-based strategy is

$$2 \times 6 \times \text{total number of element}$$

when the Whitney element is used, and

$$2 \times 3 \times \text{number of DOF on } K \times \text{total number of element}$$

when nodal elements are used. To overcome this issue, we do not assemble the global matrix coming from (22). We solve (22) on each element and use a Jacobi iterative method to ensure the convergence of the global numerical solution. We also take advantage of the natural parallelization of the DG methods to reduce the computational time of simulations.

### C. Divergence-Free Magnetic Field Constraint

The divergence-free magnetic field constraint is not satisfied explicitly. As in [34], we expect that the order of convergence of the divergence-free constraint to be  $r$  where  $r$  is the degree of the piecewise polynomials used as shape functions. In order to measure the global divergence, we use the semi-norm  $\|\mathbf{H}\|_{*,h}$  as a norm of  $\nabla \cdot \mathbf{H}$  as proposed in [35]. For a vector field  $\mathbf{H}$  that is smooth in each element  $K$  of the discrete domain, the norm of the divergence of  $\mathbf{H}$  is given by

$$\|\mathbf{H}\|_{*,h} = \sum_f \int_f \|[\mathbf{H} \cdot \mathbf{n}]\| ds + \sum_K \int_K |\nabla \cdot \mathbf{H}| dK \quad (23)$$

where  $f$  is the triangular faces of the discrete domain. The norm (23) is used to verify the convergence of the divergence of the discrete magnetic field.

## IV. NUMERICAL EXAMPLES

### A. Problem With a Manufactured Solution

In order to verify the order of convergence of the local DG-based strategy using different elements, we use a constant resistivity of one. In this case, the resulting system of equations is a Friedrichs' system and the theory of such systems can, therefore, be used. To ease the computation of the error, the manufactured solution technique is used. For a magnetic field given by

$$\mathbf{H} = (\sin(3\pi(y+z)), \cos(2\pi(x+z)), \sin(\pi(x+y))) e^{-t}$$

the corresponding source term  $\mathbf{F}$  and the electric field  $\mathbf{E}$  are computed so that  $\mathbf{H}$  is a solution of system (5). The magnetic field  $\mathbf{H}$  and the electric field  $\mathbf{E}$  are imposed on all  $\Gamma$ . The magnetic permeability  $\mu$  is set to 1. The geometry is a unit cube. Quasi-uniform meshes with tetrahedral elements are used. The mesh grid size is denoted by  $h$ . The time interval is  $I = [0, 0.1]$  and the time-step size is chosen between 0.0025 and 0.01 in such a way that the error associated with the time scheme is dominated by the error associated with the FEM discretization. The fixed-point iterations are considered to converge when the Euclidean norm of the residual and of the relative correction of the discrete problem are, respectively, less than  $\delta_r = 10^{-6}$  and  $\delta_c = 10^{-5}$ . The shape functions, for each dependent variable, correspond to those associated with the Whitney element (N1) or are either linear (P1) or quadratic (P2) polynomials for nodal elements. The combinations of shape functions used for the discretization of  $\mathbf{H}-\mathbf{E}$  are the P1-P1, the P2-P2, and the N1-N1 elements.

The error on the discrete magnetic field and the discrete electric field is computed using the vectorial  $L_2$ -norm (12). The convergence plots are shown in Fig. 1. The order of convergence of  $\mathbf{H}_h$  and  $\mathbf{E}_h$  are  $r+1$ , where  $r$  is the degree of polynomials used as shape functions ( $r=1, 2$  in our case), as expected for quasi-uniform meshes (cf., [33, Theorem 7.19]). Using the norm  $\|\cdot\|_{*,h}$ , we also observe a linear and a quadratic convergence of the divergence of the discrete magnetic field for P1-P1 element and for P2-P2 element. For N1-N1 element, a linear convergence for the discrete electric field  $\mathbf{E}_h$  is observed as expected from the error associated with the interpolation operator of the Whitney element [36]. For the discrete magnetic field  $\mathbf{H}_h$ , the observed order of convergence is 1.5, which is better than expected, but still in agreement with the theory. The convergence order of the divergence of the discrete magnetic field is quadratic, but we do not have theoretical results to support our numerical results.

### B. Magnetic Front Problem

For eddy currents problems, a variation of the magnetic field induces an electric current. As mentioned earlier, these problems are nonlinear when the exponent of power law (9) is  $p > 1$ . To the best of our knowledge, no analytic solutions are known for these problems in three space dimensions. However, for Bean's model, the magnetic field  $\mathbf{H}$  and the current density  $\mathbf{J}$  are known for cylindrical or rectangular geometries. In cylindrical coordinates, the  $\theta$ -component of  $\mathbf{H}$  is a continuous

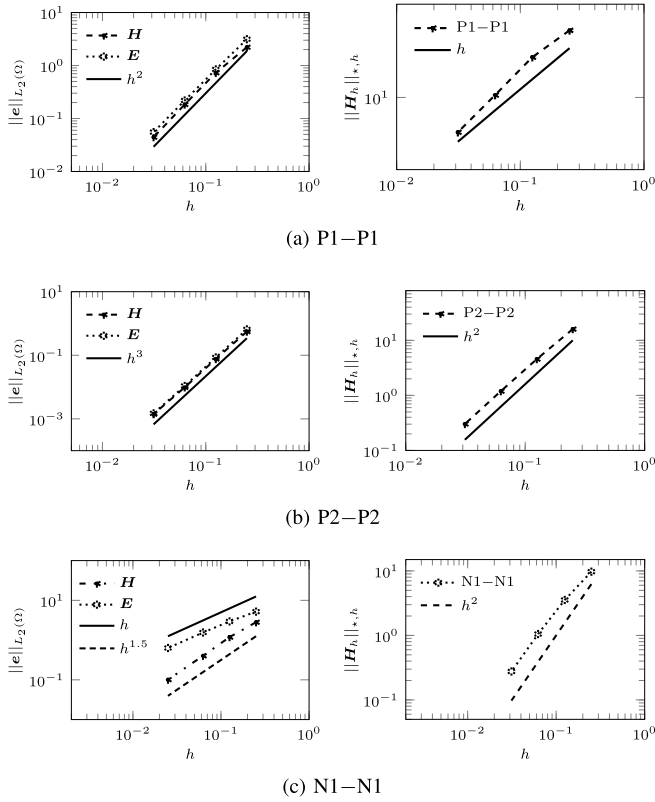


Fig. 1. Convergence plots for the problem with a manufactured solution for linear, quadratic, and the Whitney elements. (a) P1–P1. (b) P2–P2. (c) N1–N1.

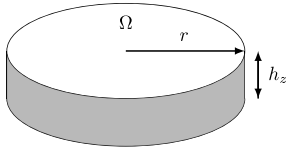


Fig. 2. Geometry for the magnetic front problem where  $h_z = 0.1$  and  $r = 1$ .

piecewise linear function and the  $z$ -component of  $\mathbf{J}$  contains a Heaviside step function [37]. Both the magnetic field and the current density penetrate the domain from the outside in. For sufficiently large values of  $p$ , the analytic solution of Bean's model is used to verify the proposed numerical methodology for nonlinear electrical resistivity (9). The magnetic front problem is also used to compare the proposed numerical strategy and the discretization of the  $\mathbf{H}$  formulation using the GFEM with the Whitney element. We assess the final time that can be reached for a given time-step size for different values of the exponent  $p$ .

The geometry under study consists of a cylindrical superconductor of radius  $r = 1$  and height  $h_z = 0.1$ , illustrated in Fig. 2. Larger values of  $h_z$  do not influence the observed results. The physical parameters for this paper are  $\mu = 1$ ,  $E_c = 1$ , and  $J_c = 1$ . Symmetric boundary conditions are imposed on the top and bottom of the cylinder. For the electric field, we also impose symmetric boundary conditions on the lateral area of the cylinder. Dirichlet boundary conditions are expressed in cylindrical coordinates to simplify their expression and are given by

$$\mathbf{H}(r = 1, \theta, z, t) = (H_r, H_\theta, H_z) = (0, -t, 0)$$

TABLE I  
NUMBER OF DOF FOR BOTH NUMERICAL STRATEGIES ASSOCIATED WITH THE UNSTRUCTURED MESH COMPOSED OF 1 304 079 ELEMENTS

Variable	FE discretization		
	GFEM	DG	
	Whitney	Nodal	Whitney
$\mathbf{H}$	1,660,187	15,648,948	7,824,474
$\mathbf{E}$	-	15,648,948	7,824,474
Total	1,660,187	31,297,896	15,648,948

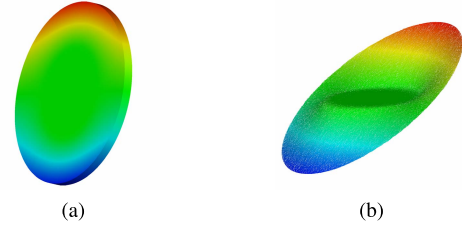


Fig. 3.  $x$ -component of the magnetic field for  $p = 10$  at  $t = 0.34$  using the proposed local DG-based strategy with the Whitney element for the magnetic front problem. The color scale from blue to red is  $[-0.35, 0.35]$ . (a)  $x$ -component of  $\mathbf{H}$  in the cylindrical geometry. (b) Graph of the  $x$ -component of  $\mathbf{H}$ .

on the lateral area of the cylinder. The initial conditions are given by  $\mathbf{H}(\mathbf{x}, 0) = 0$  and  $\mathbf{E}(\mathbf{x}, 0) = 0$ .

We first compare the proposed local DG-based strategy with the GFEM-based strategy. For a given time-step size  $\Delta t$ , we want to find the time  $t_{\max}$  such that the convergence of the fixed-point iteration scheme is lost for  $t > t_{\max}$ . The unstructured mesh is composed of 1,304,079 elements. The mesh grid size is 0.01. The nodal P1–P1 element and the Whitney element N1–N1 are used for the local DG formulation (21) and the Whitney element is used with the  $\mathbf{H}$  formulation (6) discretized with the GFEM. The number of DOF for both numerical strategies associated with the unstructured mesh is given in Table I. The tolerances are set to  $\delta_r = \delta_c = 10^{-4}$  (cf., Section IV-A). Table II gives the values of  $t_{\max}$  for which the convergence of the fixed-point iteration scheme is lost for  $t > t_{\max}$  for three different constant time-step sizes ( $\Delta t \in \{5 \times 10^{-3}, 10^{-3}, 10^{-4}\}$ ) and different values of the power-law's exponent ( $p \in \{3, 10, 50\}$ ). As the exponent increases, we see that a smaller time-step size allows the different numerical strategies to converge for a longer time interval. It is also observed that a larger time-step size can be used over a longer time interval with the proposed DG-based strategy, particularly, when we use the Whitney element. The use of very small time-step size is a well-known limitation of numerical codes used for modeling HTS and makes it difficult to model industrial scale problems. From this point of view, the proposed local DG-based strategy seems promising to overcome this issue. However, the large number of DOF makes unavoidable the use of a parallel implementation for large-scale tridimensional problems.

Using the DG-based strategy with the Whitney element, the  $x$ -component of the magnetic field  $H_x$  is illustrated for  $p = 10$  in Fig. 3. The  $y$ -component of  $\mathbf{H}$  is similar to  $H_x$  but

TABLE II

VALUES OF  $t_{\max}$  FOR WHICH THE CONVERGENCE OF THE FIXED-POINT ITERATION SCHEME IS LOST FOR  $t > t_{\max}$  FOR THREE DIFFERENT CONSTANT TIME-STEP SIZES AND DIFFERENT EXPONENTS FOR BOTH NUMERICAL STRATEGIES, FOR THE MAGNETIC FRONT PROBLEM

$\Delta t$	$p$	FE discretization	Element	$t_{\max}$ ( $\times 10^{-3}$ )
$5 \times 10^{-3}$	3	GFEM	Whitney	0
		DG	Nodal Whitney	60.0 310.0
	10	GFEM	Whitney	0
		DG	Nodal Whitney	10.0 30.0
	50	GFEM	Whitney	0
		DG	Nodal Whitney	10.0 15.0
$10^{-3}$	3	GFEM	Whitney	0
		DG	Nodal Whitney	247.0 > 500.0
	10	GFEM	Whitney	1.0
		DG	Nodal Whitney	15.0 135.0
	50	GFEM	Whitney	1.0
		DG	Nodal Whitney	12.0 18.0
$10^{-4}$	3	GFEM	Whitney	2.0
		DG	Nodal Whitney	> 500.0 > 500.0
	10	GFEM	Whitney	1.7
		DG	Nodal Whitney	336.5 > 500.0
	50	GFEM	Whitney	1.7
		DG	Nodal Whitney	16.6 220.5

with a rotation of  $90^\circ$  around the  $z$ -axis.  $H_z$  is of the order of  $10^{-3}$  and, therefore, not illustrated. As expected,  $\mathbf{H}$  and  $\mathbf{J}$  are penetrating the cylinder from the outside in, in the radial direction. The evolution of the  $z$ -component of the current density  $J_z$  is shown in Fig. 4(a) and (c) for  $p = 10$  and  $p = 50$  with a mesh grid size of  $h = 0.05$ . When  $p$  increases, the variation of the current density  $\mathbf{J}$  is sharper and closer to the solution provided by Bean's model. However, there are spurious oscillations and over-shoots (values over 0) around the sharp gradients of the current density. Fig. 4(b) illustrates the  $z$ -component of the current density for  $p = 10$  with a finer mesh grid ( $h = 0.01$ ). As the mesh is refined, we observe that the spurious oscillations diminish and the sharp gradient of the current density  $\mathbf{J}$  is better captured. Fig. 5 illustrates the order of convergence of the divergence of  $\mathbf{H}_h$  using the norm (23) for  $p = 3$  and  $p = 10$ . For both values of the exponent  $p$ , the time-step size is chosen such that we obtain convergence until  $t = 0.5$ . The convergence of the divergence of the discrete magnetic field does not guarantee that the approximations converge to the "good" solution. However, we do know that they converge to a divergence-free magnetic field solution. The order of convergence of  $\nabla \cdot \mathbf{H}_h$  when we use the Whitney element is 1.5 for  $p = 3$  and  $p = 10$ . For

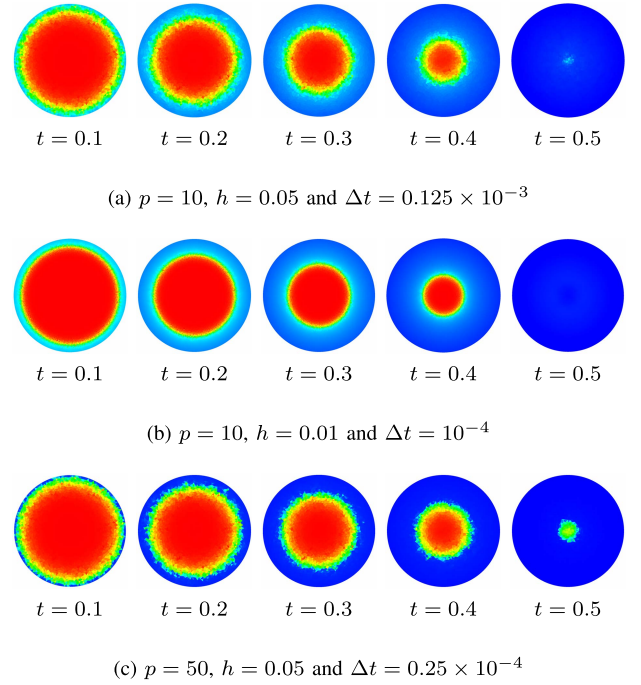


Fig. 4. Evolution of the  $z$ -component of the current density  $\mathbf{J}$  at various time steps for different mesh grid sizes and exponents  $p$  using the proposed local DG-based strategy with the Whitney element for the magnetic front problem. The color scale from blue to red is  $[-1, 0]$ . (a)  $p = 10$ ,  $h = 0.05$ , and  $\Delta t = 0.125 \times 10^{-3}$ . (b)  $p = 10$ ,  $h = 0.01$ , and  $\Delta t = 10^{-4}$ . (c)  $p = 50$ ,  $h = 0.05$ , and  $\Delta t = 0.25 \times 10^{-4}$ .

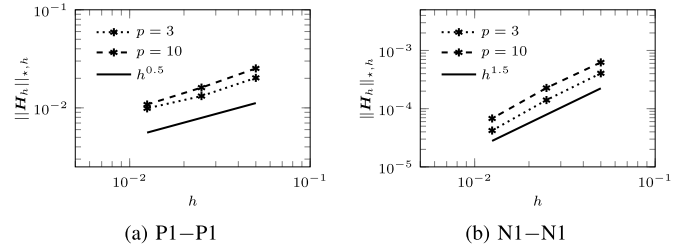


Fig. 5. Convergence plot for the error of the divergence of the discrete magnetic field using the proposed local DG strategy with the linear nodal element and the Whitney element for the magnetic front problem. (a) P1-P1. (b) N1-N1.

the local DG-based strategy with the linear nodal element, we also observe the convergence of the divergence of the discrete magnetic field. However, the order of convergence is 0.5 for both exponents. For the local DG-based strategy, the Whitney element seems to be more appropriate than the nodal element P1-P1 since it has less DOF, allows the use of a larger time-step size, and has a better convergence of the divergence of the discrete magnetic field.

### C. Magnetization of HTS Wires

The magnetization of a wire consists in exposing a wire to an external magnetic field that varies with respect to time. An electric current is then induced within the wire. In this problem, we also consider air medium around the HTS wire. Assuming that  $\sigma = 0$  in air medium, we use the following

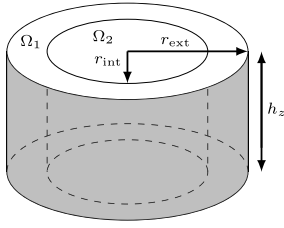


Fig. 6. Geometry of the domain for the magnetization of a circular HTS wire where  $h_z = 0.5$  mm,  $r_{\text{ext}} = 0.75$  mm, and  $r_{\text{int}} = 0.5$  mm.

model:

$$\begin{aligned}\mu \partial_t \mathbf{H} + \nabla \times \mathbf{E} &= 0 \\ \nabla \times \mathbf{H} &= 0 \\ \nabla \cdot \mathbf{H} &= 0 \\ \nabla \cdot \mathbf{E} &= 0\end{aligned}$$

which can be discretized with the proposed local DG formulation (20) with  $\sigma(\mathbf{E}_h) = 0$ . The assumption of  $\sigma = 0$  in air medium is not possible when the  $\mathbf{H}$  formulation is discretized using the GFEM with the Whitney element. We, therefore, focus on the proposed local DG-based strategy.

1) *Circular HTS Wire*: The geometry of the domain  $\Omega$  is a cylinder of radius  $r_{\text{ext}} = 0.75$  mm and height  $h_z = 0.5$  mm containing another cylinder of radius  $r_{\text{int}} = 0.5$  mm, denoted  $\Omega_2$  (cf., Fig. 6). The inner cylinder is the conducting medium and  $\Omega_1 = \Omega \setminus \Omega_2$  is the surrounding medium, which is air medium in our case. The properties of the MgB<sub>2</sub> superconductor are characterized by  $\mu = 4\pi \times 10^{-7}$  N/A<sup>2</sup>,  $E_c = 10^{-4}$  V/m,  $J_c = 10^8$  A/m<sup>2</sup>, and  $p = 50$  [38]. The quantities of reference used are  $E_0 = 1$  V/m,  $\mu_0 = 4\pi \times 10^{-7}$  N/A<sup>2</sup>,  $H_0 = (4\pi)^{-1} \times 10^7$  A/m,  $\ell_0 = 10^{-3}$  m, and  $t_0 = 10^{-3}$  s. In the following, the dimensionless quantities are denoted with a tilde (“~”). The mesh is composed of 224 265 tetrahedral elements and the dimensionless mesh grid size is  $h = 0.025$ . In order to avoid interpolating material properties, the discretization of  $\Omega$  is such that each element  $K$  of the mesh belongs to only one subdomain. The dimensionless time-step size used is  $0.5 \times 10^{-3}$ . The tolerances are set to  $\delta_r = \delta_c = 10^{-4}$ . We only use the proposed local DG-based strategy with the Whitney element for this problem.

An external magnetic field of amplitude 0.1 T with a frequency of 50 Hz on the  $y$ -component of the magnetic field  $H_y$  is applied. It induces an electric current in the  $z$ -direction. The non-dimensional external magnetic field, given by

$$\tilde{\mathbf{H}}(\tilde{\mathbf{x}}, \tilde{t}) = (0, 0.1 \sin(\pi 10^{-1} \tilde{t}), 0) \quad (24)$$

is imposed on the lateral area of the outer cylinder  $\Omega_1$ . Symmetry boundary conditions are imposed on the top and bottom of the cylinder  $\Omega$ . For the electric field, we also impose symmetry boundary conditions on the lateral area of the outer cylinder. The initial conditions are given by  $\tilde{\mathbf{H}}(\tilde{\mathbf{x}}, 0) = 0$  and  $\tilde{\mathbf{E}}(\tilde{\mathbf{x}}, 0) = 0$ .

The analytic solution provided by Bean’s model is used to verify the proposed methodology for large values of  $p$ . According to Bean’s model, the magnetic field  $\mathbf{H}$  and the current density  $\mathbf{J}$  penetrate the wire from the outside in,

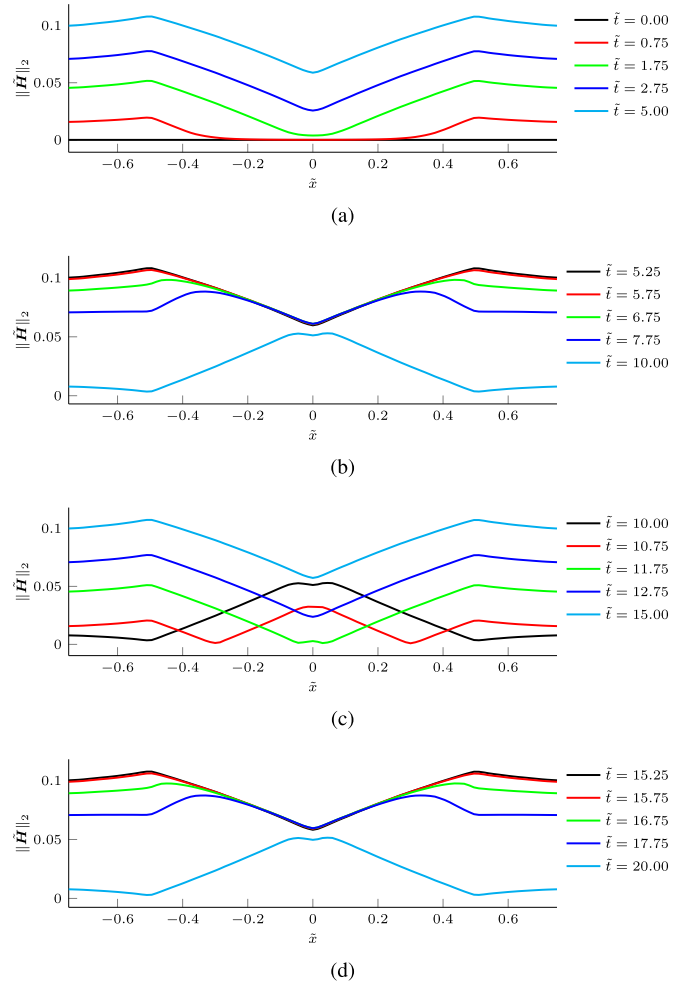


Fig. 7. Evolution of the Euclidean norm of the dimensionless magnetic field  $\mathbf{H}$  at various time steps along the  $\tilde{x}$ -axis at  $\tilde{y} = 0$  and  $\tilde{z} = 0.25$  using the proposed local DG-based strategy with the Whitney element for the magnetization of a circular HTS wire.

along the  $r$ -axis [37]. The magnetic field and the current density first get smaller as they penetrate further in the wire until they reach zero. The magnetic field then increases and penetrates further into the wire until the two fronts join at the center of the superconductor. The value of the magnetic field at the center of the wire then gets larger as illustrated in Fig. 7(a) and (c). As the amplitude of the external magnetic field decreases, we observe a remanent magnetic field in the wire, as illustrated in Fig. 7(b) and (d). Fig. 8 illustrates the dimensionless  $z$ -component of the current density at various time steps along the  $\tilde{x}$ -axis.  $\tilde{J}_z$  penetrates the wire until the two fronts meet. Fig. 9 illustrates the graph of  $\tilde{J}_z$  at  $\tilde{z} = 0.25$  when the two fronts form almost a discontinuity at the center of the wire for the first and third quarter of the period of the external magnetic field. The sharp gradients of  $\tilde{J}_z$  are captured with limited spurious oscillations. We also observe that the order of magnitude of the dimensionless  $z$ -component of the current density in air medium is about  $10^{-4}$ .

2) *Rectangular HTS Wire*: The geometry is a rectangular wire centered at  $(0, 0, 0)$  completely surrounded by air medium, as illustrated in Fig. 10, to simulate the calibration



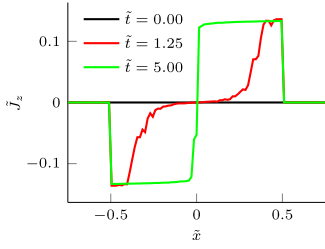


Fig. 8. Evolution of the  $z$ -component of the dimensionless current density  $\tilde{J}_z$  at various time steps along the  $\tilde{x}$ -axis at  $\tilde{y} = 0$  and  $\tilde{z} = 0.25$  using the proposed local DG-based strategy with the Whitney element for the magnetization of a circular HTS wire.

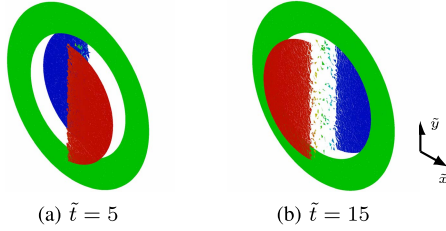


Fig. 9. 2-D slice of the dimensionless  $z$ -component of the current density  $\tilde{J}_z$  at various time steps at  $\tilde{z} = 0.25$  with  $h = 0.025$  and  $\Delta t = 0.5 \times 10^{-3}$  using the proposed local DG-based strategy with the Whitney element for the magnetization of a circular HTS wire. The color scale from blue to red is  $[-0.135, 0.135]$ . (a)  $\tilde{t} = 5$ . (b)  $\tilde{t} = 15$ .

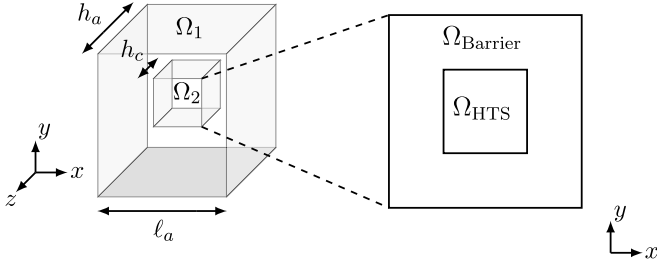


Fig. 10. Geometry of the domain for the magnetization of a square HTS wire where  $h_a = 1.0$  mm,  $h_c = 0.5$  mm, and  $l_a = 1.5$  mm.

free method that is used to measure the ac loss [39]. The wire is composed of two materials: MgB<sub>2</sub> and Nb (barrier) as in [40]. We then have  $\Omega_{\text{Barrier}} = \Omega_2 \setminus \Omega_{\text{HTS}}$ . The dimensions of the cross section of the wire are:  $0.698 \times 0.680$  mm<sup>2</sup> for the HTS and  $1.170 \times 1.140$  mm<sup>2</sup> for the barrier. We consider the temperature at 27 K. The properties of Nb are then  $\mu_{\text{Nb}} = 4\pi \times 10^{-7}$  N/A<sup>2</sup> and  $\rho_{\text{Nb}} = 0.638 \times 10^{-8}$   $\Omega$ m [41]. The MgB<sub>2</sub> is characterized by the same properties than in Section IV-C1, except for  $p = 109$  and  $J_c = \frac{I_c}{A}$ , where  $I_c = 177$  A is the critical current and  $A$  is the surface area of the cross section of the superconducting material in the wire [38]. The quantities of reference are chosen as in Section IV-C1. For Nb, we also choose  $\rho_0 = \rho_{\text{Nb}}$ .

The external magnetic field is given by

$$\mathbf{H}(\mathbf{x}, t) = (0, 0.1 \sin(2\pi f t), 0)$$

where  $f = 144$  Hz is the frequency and is imposed on the faces of  $\Omega_1$  that are parallel either to the  $xy$  plane or  $yz$  plane. Symmetry boundary conditions are imposed on the

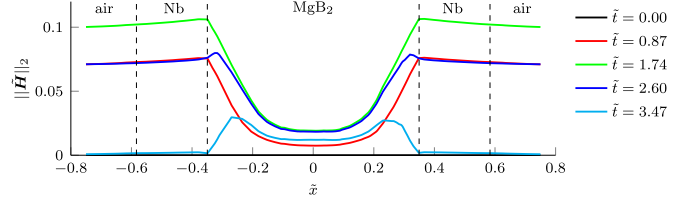


Fig. 11. Evolution of the Euclidean norm of the dimensionless magnetic field  $\mathbf{H}$  at various time steps along the  $\tilde{x}$ -axis at  $\tilde{y} = 0.57$  and  $\tilde{z} = 0.25$  using the proposed local DG-based strategy with the Whitney element for the magnetization of a rectangular HTS wire.

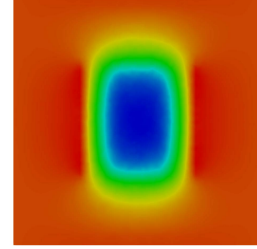


Fig. 12.  $y$ -component of the dimensionless magnetic field  $\tilde{H}_y$  on the  $xy$  plane at  $\tilde{z} = 0.25$  and  $\tilde{t} = 1.74$  using the proposed local DG-based strategy with the Whitney element for the magnetization of a rectangular HTS wire. The color scale from blue to red is  $[0.02, 0.11]$ .

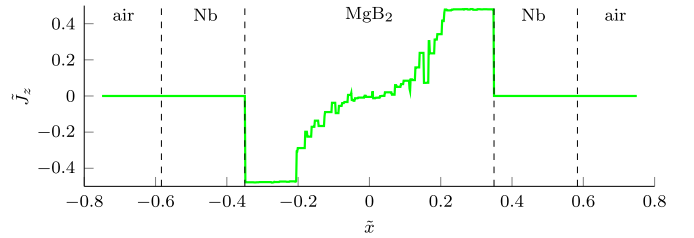


Fig. 13.  $z$ -component of the dimensionless current density  $\tilde{J}_z$  along the  $\tilde{x}$ -axis at  $\tilde{y} = 0.57$ ,  $\tilde{z} = 0.25$ , and  $\tilde{t} = 1.74$  using the proposed local DG-based strategy with the Whitney element for the magnetization of a rectangular HTS wire.

other faces for  $\mathbf{H}$ . For the electric field, we impose symmetry boundary conditions on all faces of  $\Omega_1$ . The initial conditions are  $\mathbf{H}(\mathbf{x}, 0) = 0$  A/m and  $\mathbf{E}(\mathbf{x}, 0) = 0$  V/m. The mesh is composed of 293 048 tetrahedral elements. The dimensionless mesh grid size in  $\Omega_1$  and in  $\Omega_2$  are given, respectively, by  $h_{\Omega_1} = 0.05$  and  $h_{\Omega_2} = 0.025$ . As for the magnetization of a circular HTS wire, the discretization of the domain is such that each element  $K$  of the mesh belongs to only one subdomain. The non-dimensional time-step size is  $\Delta t = 0.1 \times 10^{-3}$ . The tolerances are set to  $\delta_r = \delta_c = 10^{-4}$ . Only the Whitney element is used.

Figs. 11 and 12 illustrate, respectively, the norm of the dimensionless magnetic field for various time steps in the first half of the period of the external magnetic field, and  $\tilde{H}_y$  on the  $xy$  plane at  $\tilde{z} = 0.25$  and  $\tilde{t} = 1.74$ . As for the magnetization of a cylindrical HTS wire, the numerical results are in agreement with Bean's model solutions, which are similar to what we describe in Section IV-C1, for a rectangular HTS wire. Fig. 13 illustrates the  $z$ -component of the dimensionless current density along the  $\tilde{x}$ -axis at  $\tilde{y} = 0.57$ ,

$\tilde{z} = 0.25$ , and  $\tilde{t} = 1.74$ . The sharp gradients of the current density are captured with limited induced spurious oscillations and the order of magnitude of  $\tilde{J}_z$  in Nb and air medium are, respectively, about  $10^{-4}$  and  $10^{-5}$ . As expected, there are strong eddy currents in the HTS.

## V. CONCLUSION

A numerical strategy is proposed to use a local DG method to discretize a low-frequency approximation to Maxwell's equations, with a nonlinear electrical resistivity, for modeling high-temperature superconductor problems. A linear upwind-like numerical flux is proposed using the inverse function of Ohm's law. In order to verify the implementation of the local DG strategy with different elements, we use a constant resistivity of one. The order of convergence of the discrete-dependent variables for a problem with a known solution is verified using either the theory of the DG method applied on Friedrichs' systems or the error associated with the interpolation operator of the Whitney element. The magnetic front problem with a nonlinear electrical resistivity is used to verify the local DG-based strategy for HTS modeling. A comparison between the proposed strategy and the  $\mathbf{H}$  formulation discretized using the GFEM with the Whitney element is performed based on the final time that can be reached for a given time-step size for different values of the power-law's exponent. For large values of the exponent  $p$  in the power-law model of the electrical resistivity, the time-step size must be smaller to reach a larger final time, but it is observed that a larger time-step size can be used over a longer time interval with the proposed DG-based strategy, particularly, when we use the Whitney element. For the local DG-based strategy with the Whitney element, the sharp gradients of the current density have been captured with limited numerically induced oscillations for both the magnetic front problem and the magnetization of HTS wires.

## ACKNOWLEDGMENT

The authors would like to thank Prof. F. Sirois for introducing them to this topic and for his helpful comments on this paper. They would also like to thank Prof. M. Laforest and Prof. S. Prudhomme for their interesting and helpful conversations. Parts of this research are based on the Ph.D. thesis of the first author [42]. This work was supported by the Fonds de recherche du Québec - Nature et technologies (FRQNT).

## REFERENCES

- [1] R. Brambilla, F. Grilli, and L. Martini, "Development of an edge-element model for AC loss computation of high-temperature superconductors," *Supercond. Sci. Technol.*, vol. 20, no. 1, pp. 16–24, 2006.
- [2] J. K. Sykulski, R. L. Stoll, A. E. Mahdi, and C. P. Please, "Modelling HTc superconductors for AC power loss estimation," *IEEE Trans. Magn.*, vol. 33, no. 2, pp. 1568–1571, Mar. 1997.
- [3] N. Amemiya, K. Miyamoto, N. Banno, and O. Tsukamoto, "Numerical analysis of AC losses in high Tc superconductors based on E-J characteristics represented with n-value," *IEEE Trans. Appl. Supercond.*, vol. 7, no. 2, pp. 2110–2113, Jun. 1997.
- [4] N. Amemiya, S.-I. Murasawa, N. Banno, and K. Miyamoto, "Numerical modelings of superconducting wires for AC loss calculations," *Phys. C, Supercond.*, vol. 310, nos. 1–4, pp. 16–29, Dec. 1998.

- [5] Y.-M. Law and M. Laforest, "A nonlinear relaxation formulation of the p-curl problem modelling high-temperature superconductors: A modified Yee's scheme," *J. Comput. Phys.*, vol. 378, pp. 591–614, Feb. 2019.
- [6] A. Kameni, J. Lambrechts, J.-F. Remacle, S. Mezani, F. Bouillault, and C. Geuzaine, "Discontinuous Galerkin method for computing induced fields in superconducting materials," *IEEE Trans. Magn.*, vol. 48, no. 2, pp. 591–594, Feb. 2012.
- [7] I. D. Mayergoyz, *Nonlinear Diffusion of Electromagnetic Fields: With Applications to Eddy Currents and Superconductivity*. San Diego, CA, USA: Academic, 1998.
- [8] F. Sirois and F. Grilli, "Numerical considerations about using finite-element methods to compute AC losses in HTScs," *IEEE Trans. Appl. Supercond.*, vol. 18, no. 3, pp. 1733–1742, Sep. 2008.
- [9] F. Sirois and F. Grilli, "Potential and limits of numerical modelling for supporting the development of HTS devices," *Supercond. Sci. Technol.*, vol. 28, no. 4, 2015, Art. no. 043002.
- [10] S. Ausserhofer, O. Biro, and K. Preis, "Discontinuous Galerkin finite elements in time domain eddy-current problems," *IEEE Trans. Magn.*, vol. 45, no. 3, pp. 1300–1303, Mar. 2009.
- [11] J. Smajic, M. Bucher, R. Christen, and Z. Tanasic, "DG-FEM for time domain H- $\phi$  eddy current analysis," *IEEE Trans. Magn.*, vol. 53, no. 6, Jun. 2017, Art. no. 7202604.
- [12] J. Smajic, M. Bucher, R. Christen, and Z. Tanasic, "Stability analysis of time domain discontinuous Galerkin H- $\phi$  method for eddy current simulations," *IEEE Trans. Magn.*, vol. 54, no. 3, Mar. 2018, Art. no. 7204404.
- [13] E. Blank, "The discontinuous Galerkin method for Maxwell's equations: Application to bodies of revolution and Kerr-nonlinearities," Ph.D. dissertation, Karlsruhe Inst. Technol., Karlsruhe, Germany, 2013.
- [14] V. A. Bokil, Y. Cheng, Y. Jiang, and F. Li, "Energy stable discontinuous Galerkin methods for Maxwell's equations in nonlinear optical media," *J. Comput. Phys.*, vol. 350, pp. 420–452, Dec. 2017.
- [15] J. Huang and C.-W. Shu, "A second-order asymptotic-preserving and positivity-preserving discontinuous Galerkin scheme for the Kerr–Debye model," *Math. Models Methods Appl. Sci.*, vol. 27, no. 3, pp. 546–579, 2017.
- [16] A. Kameni, M. Boubekeur, L. Alloui, F. Bouillault, J. Lambrechts, and C. Geuzaine, "A 3-D semi-implicit method for computing the current density in bulk superconductors," *IEEE Trans. Magn.*, vol. 50, no. 2, pp. 377–380, Feb. 2014.
- [17] L. Makong, A. Kameni, P. Masson, J. Lambrechts, and F. Bouillault, "3-D modeling of heterogeneous and anisotropic superconducting media," *IEEE Trans. Magn.*, vol. 52, no. 3, Mar. 2016, Art. no. 7205404.
- [18] L. Makong, A. Kameni, F. Bouillault, C. Geuzaine, and P. Masson, "Nodal discontinuous Galerkin method for high-temperature superconductors modeling based on the H-formulation," *Int. J. Numer. Model.*, vol. 31, no. 2, Mar./Apr. 2018, Art. no. e2298.
- [19] K. Berger, J. Leveque, D. Netter, B. Douine, and A. Rezzoug, "AC transport losses calculation in a Bi-2223 current lead using thermal coupling with an analytical formula," *IEEE Trans. Appl. Supercond.*, vol. 15, no. 2, pp. 1508–1511, Jun. 2005.
- [20] D. Hu *et al.*, "DC characterization and 3D modelling of a triangular, epoxy-impregnated high temperature superconducting coil," *Supercond. Sci. Technol.*, vol. 28, no. 6, 2015, Art. no. 065011.
- [21] V. M. R. Zermeno, F. Grilli, and F. Sirois, "A full 3D time-dependent electromagnetic model for Roebel cables," *Supercond. Sci. Technol.*, vol. 26, no. 5, 2013, Art. no. 052001.
- [22] A. Bossavit, *Computational Electromagnetism: Variational Formulations, Complementarity, Edge Elements*. San Diego, CA, USA: Academic, 1998.
- [23] W. Paul, D. Hu, and T. Baumann, "Voltage-current characteristic between  $10^{-13}$  V/cm and  $10^{-3}$  V/cm of BSCCO and time decay of the magnetization," *Phys. C, Supercond.*, vols. 185–189, pp. 2373–2374, Dec. 1991.
- [24] J. Rhyner, "Magnetic properties and AC-losses of superconductors with power law current—Voltage characteristics," *Phys. C, Supercond.*, vol. 212, nos. 3–4, pp. 292–300, 1993.
- [25] H.-M. Yin, "Regularity of weak solution to a p-curl-system," *Differ. Integral Equ.*, vol. 19, no. 4, pp. 361–368, 2006.
- [26] H.-M. Yin, B. Q. Li, and J. Zou, "A degenerate evolution system modeling Bean's critical-state type-II superconductors," *Discrete & Continuous Dyn. Syst.-A*, vol. 8, no. 3, pp. 781–794, 2002.
- [27] A. Logg, K.-A. Mardal, and G. Wells, *Automated Solution of Differential Equations by the Finite Element Method: The FEniCN book*, vol. 84. Berlin, Germany: Springer, 2012.
- [28] J.-M. Jin, *The Finite Element Method in Electromagnetics*. New York, NY, USA: Wiley, 2014.

- [29] M. Zhang and T. A. Coombs, "3D modeling of high-TC superconductors by finite element software," *Supercond. Sci. Technol.*, vol. 25, no. 1, 2011, Art. no. 015009.
- [30] G. Mur, "Edge elements, their advantages and their disadvantages," *IEEE Trans. Magn.*, vol. 30, no. 5, pp. 3552–3557, Sep. 1994.
- [31] Z. Ren, "Influence of the RHS on the convergence behaviour of the curl-curl equation," *IEEE Trans. Magn.*, vol. 32, no. 3, pp. 655–658, May 1996.
- [32] J. S. Hesthaven and T. Warburton, *Nodal Discontinuous Galerkin Methods: Algorithms, Analysis, and Applications*. New York, NY, USA: Springer, 2000.
- [33] D. A. Di Pietro and A. Ern, *Mathematical Aspects of Discontinuous Galerkin Methods*, vol. 69. Berlin, Germany: Springer, 2011.
- [34] J. S. Hesthaven and T. Warburton, "Nodal high-order methods on unstructured grids: I. Time-domain solution of Maxwell's equations," *J. Comput. Phys.*, vol. 181, no. 1, pp. 186–221, 2002.
- [35] B. Cockburn, F. Li, and C.-W. Shu, "Locally divergence-free discontinuous Galerkin methods for the Maxwell equations," *J. Comput. Phys.*, vol. 194, no. 2, pp. 588–610, Mar. 2004.
- [36] J.-C. Nédélec, "Mixed finite elements in  $R^3$ ," *Numer. Math.*, vol. 35, no. 3, pp. 315–341, 1980.
- [37] C. P. Bean, "Magnetization of high-field superconductors," *Rev. Mod. Phys.*, vol. 36, no. 1, pp. 31–39, 1964.
- [38] K. Kajikawa *et al.*, "AC losses in monofilamentary MgB<sub>2</sub> round wire carrying alternating transport currents," *Supercond. Sci. Technol.*, vol. 23, no. 4, 2010, Art. no. 045026.
- [39] J. Šouc, F. Gömöry, and M. Vojenciak, "Calibration free method for measurement of the AC magnetization loss," *Supercond. Sci. Technol.*, vol. 18, no. 5, pp. 592–595, 2005.
- [40] S. Safran, J. Šouc, F. Gömöry, P. Kováč, and A. Gencer, "Experimentally determined magnetization ac losses of mono and multifilamentary MgB<sub>2</sub> wires," *J. Supercond. Novel Magn.*, vol. 26, no. 5, pp. 1557–1561, 2013.
- [41] J. E. Campbell, E. A. Eldridge, and J. K. Thompson, "Handbook on Materials for Superconducting Machinery," DTIC, Fort Belvoir, VA, USA, Tech. Rep. MCIC-HB-04, 1974.
- [42] Y.-M. Law-Kam-Cio, "Methode de Galerkin discontinue pour la discretisation par elements finis des equations de Maxwell pour la modelisation de problemes d'electromagnetisme en basses frequences," Ph.D. dissertation, Ecole Polytech. Montreal, Montreal, QC, Canada, 2018.